An Elastic Triboelectric Nanogenerator for Harvesting Random Mechanical Energy with Multiple Working Modes

Yuliang Chen, Ying Zhang, Taotao Zhan, Zhiming Lin, Steven L. Zhang, Haiyang Zou, Guobin Zhang, Chongwen Zou, and Zhong Lin Wang*

Because of the shortage of fossil energy and the rapid development of Internet of things nowadays, renewable and clean energy is becoming valuable and necessary. One renewable energy source, triboelectric nano-generators (TENGs), has been proved to effectively harvest energy from vibration, walking, and even sphygmus. TENGs based on contact–separation mode are foremost and fundamental, and the input stimuli for TENGs are strictly limited by constant amplitude and uniaxial direction of motion, which limits many practical applications. Therefore, it is extremely meaningful to develop a kind of TENG to collect random energy, which ubiquitously exists in the ambient environment. Here, an elastic rubber is placed inside the structure of an elastic TENG (E-TENG). With this novel structure, the output signals of the TENG are almost independent of the amplitude of the external stimuli due to the elasticity of rubber. Moreover, the E-TENG shows good performance on angle detection without the limitation of the direction of stimuli. It is believed that the E-TENG will contribute to developing next-generation flexible TENGs and self-powered sensors in the future.

Global warming and climate change, which mainly attribute to the heavy consumption of fossil fuels, have become two of the most serious problems that the world faces for the past decades.[1] Considering the diminishing of fossil fuels, the exploration and exploitation of renewable and clean energy need to be urgently implemented. It has been proven that TENG may be a good alternative due to its effectiveness in harvesting ambient mechanical energy.[2–5] In addition, TENGs themselves can also be used as self-powered sensors, due to the converted electric signals usually vary with external stimuli. These self-powered sensors based on TENGs have been successfully applied to sense and monitor motion, vibration, environmental and biological monitoring.[6–9]

Traditionally, the operation of TENGs can be divided into four modes: vertical contact–separation mode, lateral sliding mode, single-electrode mode, and freestanding mode.[10] Among those modes, contact–separation is the most common and foremost one, based on the relative motions between two dissimilar materials. The TENGs based on contact–separation mode are usually fabricated by gluing two different polarity dielectrics on rigid substrates, respectively.[11–14] The polymer materials, e.g., nylon, polytetrafluoroethylene (PTFE) are usually selected as the dielectrics,[15–19] due to their advanced performance in triboelectric series.[20] The rigid acrylic board is easy to be cut and has chemical inertness, insulating properties, which is usually used as a substrate in the fabrication of TENGs.[6,21,22] To generate electric output, the two dissimilar materials are first forced to contact with each other, and then separated to a certain distance. During this contact–separation event, the distance between the two dissimilar dielectrics is critical. If the approaching distance is not enough to make the two dielectrics contact, the electric signals of the TENG are low, because most of the charges are not transferred by contact electrification.[23,24] Also, if the approaching distance is larger than the original separated distance of the two dielectrics, the high force due to contact may destroy the TENGs, which mean the motion amplitude and the direction of the applied stimuli are strictly limited. In contrast, irregular and random mechanical stimuli are commonly existing in the ambient environment, which may not be suitable for harvesting from traditional contact–separation TENG.

Here, an elastic rubber film between two electrodes to develop an advanced elastic TENG (E-TENG) was introduced

Y. L. Chen, Prof. Y. Zhang, Z. M. Lin, S. L. Zhang, H. Y. Zou, Prof. Z. L. Wang
School of Materials Science and Engineering
Georgia Institute of Technology
Atlanta 30332-0245, USA
E-mail: zhong.wang@mse.gatech.edu

Y. L. Chen, Prof. G. B. Zhang, Prof. C. W. Zou
National Synchrotron Radiation Laboratory
University of Science and Technology of China
Hefei 230029, China

Prof. Y. Zhang, T. T. Zhan
Key Laboratory of Thermo-Fluid Science and Engineering
Ministry of Education
Xi'an Jiaotong University
Xi'an 710049, China

Prof. Z. L. Wang
Beijing Institute of Nanoenergy and Nanosystems
Chinese Academy of Sciences
Beijing 100085, China

Prof. Z. L. Wang
College of Nanoscience and Technology
University of Chinese Academy of Sciences
Beijing 100049, China

The ORCID identification number(s) for the author(s) of this article can be found under https://doi.org/10.1002/admt.201900075.

to overcome the above challenges. Due to the elasticity of rubber, the stimuli with various amplitude and directions can be adopted in principle, because according to the working mechanism of contact–separation mode,[23] once the electrodes are contacted and separated with respect to the elastic rubber, the electric signals should be generated. In order to exhibit advanced performance, three modes, i.e., single contacting, dual contacting and rotation modes, are indicated in our experiments. The stimuli with various amplitudes are applied to our E-TENG to produce stable electric signals based on single contact or dual contact mode. The generated electrical energy by E-TENG can efficiently light up LEDs or charge a commercial energy storage device for further applications. A rotation operation mode of this E-TENG can utilize the stimuli with different directions. For example, the output signals raise with the increase of rotation angle, owing to the increasing contacting areas between the rubber and electrodes, suggesting that the E-TENG can also be used as an angle sensor. This novel design of the E-TENG with elastic dielectric can potentially be generalized to flexible TENGs that can further improve the performance of energy harvesting and self-powered sensors.

Figure 1a shows the schematic of the E-TENG. A rubber film was installed at the middle of the two copper (Cu) electrodes, which were fabricated by winding copper films around the quasi-ellipse columns. Other details of the fabrication processes are presented in the Experimental Section. The E-TENG is operated by using the contact–separation mode with the contact–separation events between the rubber and two electrodes (described as dual contacting mode) shown in Figure 1b. Owing to the elasticity of rubber, the uniaxial motion of the Cu electrodes exceeds the original distance between the electrodes and rubber, which means the TENG can work effectively without the limitation of the amplitude of the irregular stimuli. The working principle of the TENG at short-circuit condition is summarized as follows (Figure 1b). After the first contact–separation event happened between one copper electrode and the rubber triggered by external mechanical force, the copper film became positively charged and rubber turned into negatively charged according to triboelectric series.[20] Because the rubber film contacted the two Cu electrodes, both sides of the rubber film would become negatively charged. As shown in Figure 1b, i) due to the electrostatic screen effect, the positive charge assembles on the electrode which is contacted with the rubber; ii,iii) moving the electrodes to the right, would weaken the electrostatic screening effect on the electrode that was previously in contact with rubber. Then, the electrons would transfer from the electrode to the other electrode gradually with a uniaxial motion to balance the electric field; iv) when the other electrode contacts the rubber film, half of the cycle is finished, and the other half of the cycle is same as above processes.

Figure 1c shows the open-circuit voltage (V_{oc}) when external stimuli with different amplitudes (d) are applied. Because the original distance between the two electrodes is 14 mm, once the amplitude of the stimulus is beyond 14 mm, the elastic rubber would deform (Figure S1, Supporting Information). When each electrode just contacts the rubber film without causing any deformation (i.e., $d = 14$ mm) by a small force, the V_{oc} is around 70 V. The V_{oc} would increase slightly to around 85 V when greater force was applied to the rubber film causing

deformation ($d = 34$ mm), attributing to the extra contacting area from the lateral part of the electrodes and the tighter contact between electrodes and rubber film. However, when d is more than 34 mm, the V_{oc} remain constant, for instance, the V_{oc} still is around 85 V at $d = 39$ mm. Similar to the V_{oc} results, the short-circuit transferred charge (Q_{sc}) slightly increases to a saturated value (≈ 29 nC) when d is larger than 34 mm (Figure 1d). These results indicate that our TENG can keep an almost stable performance when different external stimuli are applied. The V_{oc} (Figure 1e) and short-circuit current (I_{sc}, Figure 1f) were measured at same amplitude ($d = 34$ mm), but with varying frequencies. The peak to peak amplitude of V_{oc} (ΔV_{oc}, $\Delta V_{oc} = V_{oc}$, because we set the minimum potential to be 0 V) is around 85 V when the E-TENG operates at 1–4 Hz (red dashed in Figure 1g). The bigger peak to peak amplitude of I_{sc} (ΔI_{sc}) can be produced at a higher frequency (olive dashed in Figure 1g). For example, the ΔI_{sc} reaches 1.8 μA at 4 Hz. The electric output is also affected by the external resistances. With the increase of the external resistances (R_e), the voltage across the resistor also increases, and the maximum output peak to peak voltage (V_{peak}) achieves to its peak of 118 V (59 V × 2, because only one-side peak to peak voltage during switch-on should be considered to calculate power) at 4.74×10^8 Ω (Figure 1h). It should be noted that this value is larger than the ΔV_{oc} (≈ 85 V in Figure 1g). Further investigation needs to be conducted to understand the abnormal phenomenon (Figure S2, Supporting Information). The maximum output power density (P_{peak}) based on Ohm's law can be calculated as

$$P_{peak} = \frac{V_{peak}^2}{4R_e} \tag{1}$$

and the instantaneous power density (P) reaches its maximum at a load resistance of ≈ 100 MΩ, corresponding to a peak power density of ≈ 84 mW m^{-2} (Figure 1h).

In another situation, when only one of the copper electrodes contacted the rubber (described as single contacting mode), the similar results show that the $V_{oc} = \approx 46$ V, $Q_{sc} = \approx 20$ nC, and $P_{peak} = \approx 10$ mW m^{-2} at a resistance of ≈ 100 MΩ (Figure S3, Supporting Information). Compared with the corresponding signals of the dual contacting mode, the signals of single contacting mode are lower, because only one face of the rubber is contacted with one of the copper electrodes.

The above results mainly prove the TENG's high performance subjected to the uniaxial motions with different amplitudes. In addition, since the rubber film has an outstanding elasticity, the external stimuli with different directions are expected to be available for our E-TENG. For example, the schematic of when rotation stimuli are applied to the E-TENG is shown in **Figure 2**a. The working processes are similar to the direct contact–separation mode in Figure 2b. The applied rotation changes the contact area of rubber and electrodes, which will drive electrons to transfer along the circuit to balance the electric field in the short-circuit condition. The difference is that the voltage is produced between copper electrodes and ground rather than originating from the two electrodes in dual contacting mode (Figure 1b). Since the contacting area is associated with the rotational angle, Figure 2c,d shows V_{oc} and Q_{sc} as functions of rotational angle (w) of stimuli, respectively. The

**ADVANCED
SCIENCE NEWS**

www.advancedsciencenews.com

**ADVANCED
MATERIALS
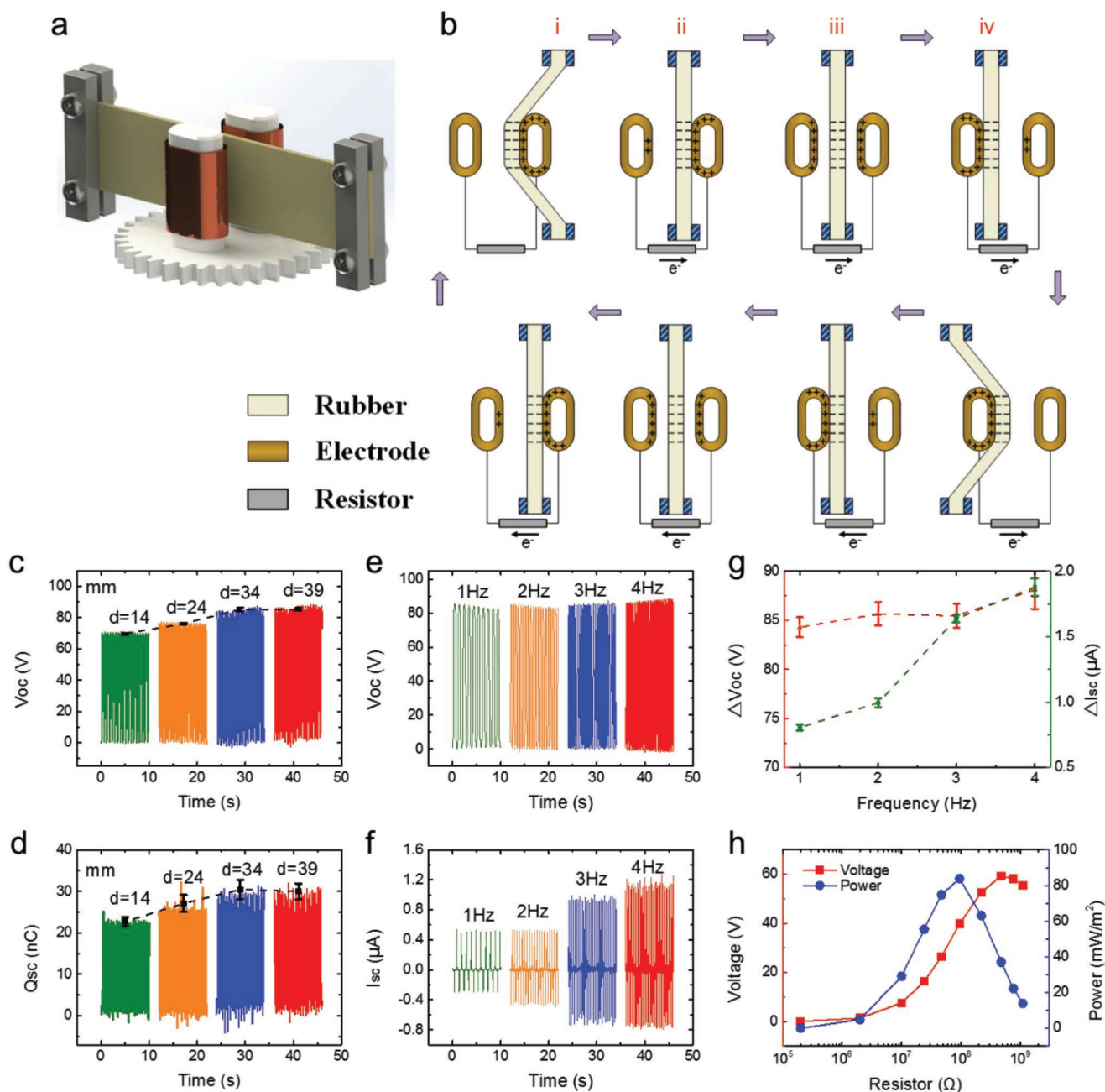TECHNOLOGIES**

www.advmattechnol.de

Figure 1. The elastic triboelectric nanogenerator (E-TENG) operates at the dual contacting mode. a) The schematic of the E-TENG. A flexible and elastic rubber is placed at the middle of two copper electrodes as one of the triboelectric layers. b) The working processes of the E-TENG based on dual contacting mode. The electric signals can be generated by the contact–separation events between the rubber and two electrodes. When the external stimuli with different amplitudes (d) are applied on the E-TENG, the open-circuit voltage (V_{oc}) c) and the short-circuit transferred charge (Q_{sc}) d) are measured. The black dashed lines are the derived amplitude of V_{oc} in (c) and Q_{sc} in (d), respectively. When the external stimuli with same amplitude (d = 34 mm) but different frequencies (f) are applied, the V_{oc} e) and the short-circuit current (I_{sc}) f) are measured, respectively. g) The red curve is the peak to peak amplitude of V_{oc} (ΔV_{oc}) derived from (e); and the green curve is the peak to peak amplitude of I_{sc} (ΔI_{sc}) derived from (f), both as functions of frequency. h) An external load is connected to the E-TENG, the red curve is the voltage with different resistances. The blue curve is the calculated peak power as a function of resistance. The applied stimulus is d = 34 mm, f = 1 Hz. All error bars represent standard deviation from independent measurements.

heart-shaped curve in Figure 2c shows the electric output (V_{oc}) at different rotational angles, from −180° to 180°. The trend observed is that with increasing rotational angle, the open-circuit potential difference increases. For example, V_{oc} is around 40 V at ±180°. The Q_{sc} also shows the same trend as V_{oc}, e.g.,

$Q_{sc} = \approx 12.5$ nC at ±180° (Figure 2d). When the rotational angle changed periodically from 0° to 80°, the V_{oc} (Figure 2e) and I_{sc} (Figure 2f) were measured at different frequencies. The results suggest the ΔV_{oc} is constant around 15 V even the frequency is up to 4 Hz (red line in Figure 2g), in contrast, the ΔI_{sc} increases
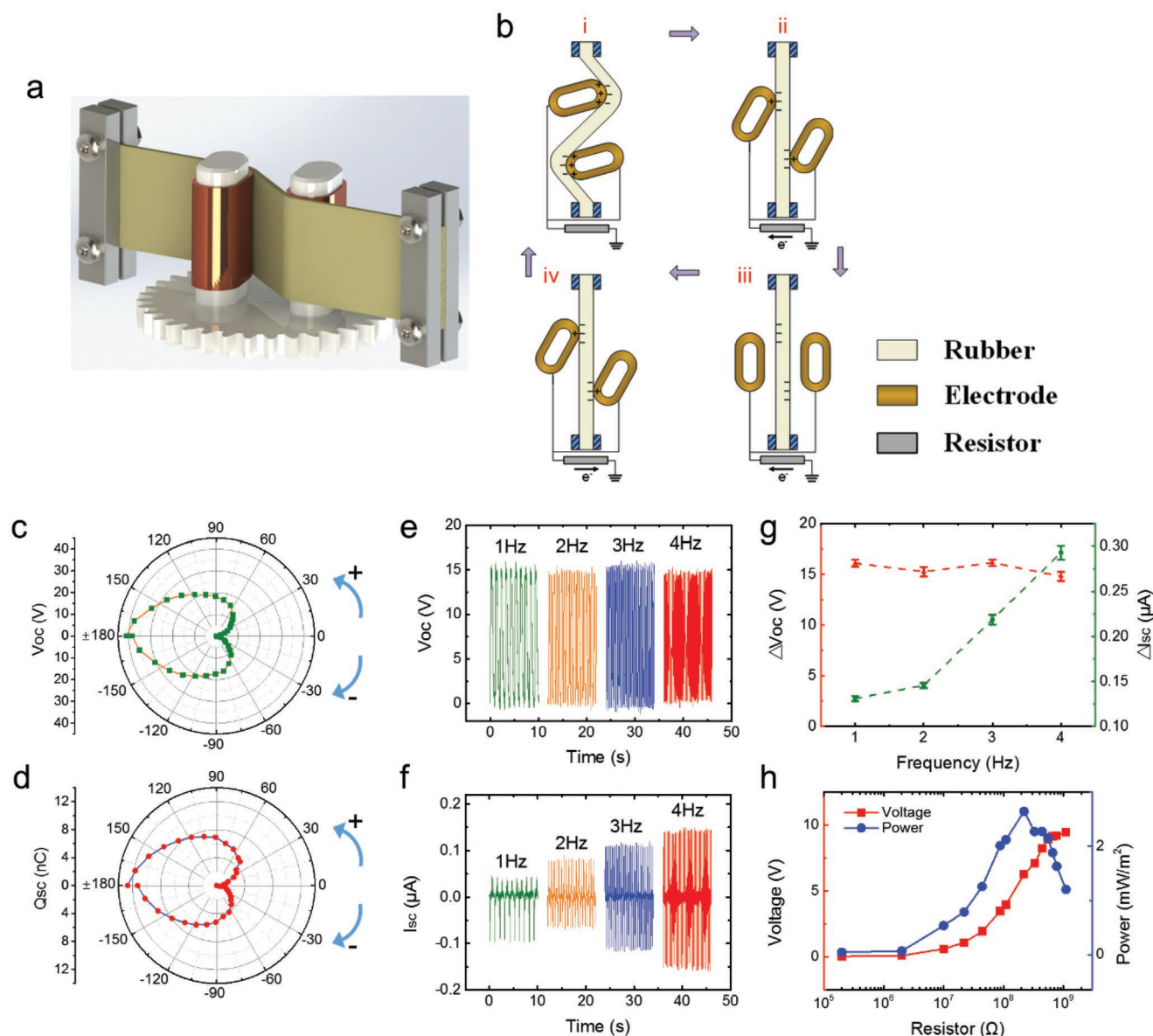
Figure 2. When the rotation mode is applied to E-TENG. a) The schematic of the E-TENG working on rotation mode. b) The working processes of the E-TENG based on rotation mode. The electric signals can be generated between the two electrodes and ground. When the external stimuli with different angles (w) are applied on the E-TENG, the V_{oc} c) and the Q_{sc} d) are measured, respectively. When the external stimuli with the same amplitude ($w = 80°$) and different frequencies (f) are applied, the V_{oc} e) and the I_{sc} f) are measured, respectively. g) The red curve is the ΔV_{oc} derived from (e) and the green curve is the ΔI_{sc} derived from (f) as a function of frequency, respectively. h) An external load is connected to the E-TENG, the red curve is the voltage on the load with different resistances. The blue curve is the calculated peak power as a function of resistance. ($w = 80°$, $f = 1$ Hz). All error bars represent standard deviation from independent measurements.

with frequency (olive line in Figure 2g). The instantaneous power density (P) reaches its maximum of around 2.13 mW m^{-2} (Figure 2h) at a load resistance of ≈110 MΩ.

Finite element analysis (FEA) is a powerful tool for electrostatic analysis. Here, the open-circuit potential of the contact–separation mode and rotation mode of the E-TENG were calculated with FEA method by COMSOL Multiphysics software (**Figure 3**), where the colors correspond to the magnitude of potential.[25] For the contact–separation mode, in Figure 3a, the electric field of the copper electrode contacting the rubber is screened, resulting in lower potential compared to the other

copper electrode. The arrows in the figure show the electric field lines. Their directions from high potential to low potential match the potential distribution. When the rubber is rightly located at the middle of the two electrodes, both electrodes have high potential (Figure 3b). For this situation, the structure is symmetric, so the two electrodes have the same potential, which could be proved by the mirror symmetry of electric field lines. At this moment, there is no output voltage between these two electrodes when they are connected by an external wire. On the other hand, for the rotation mode, the structure is always symmetric at any angle (Figure 3c,d), which means
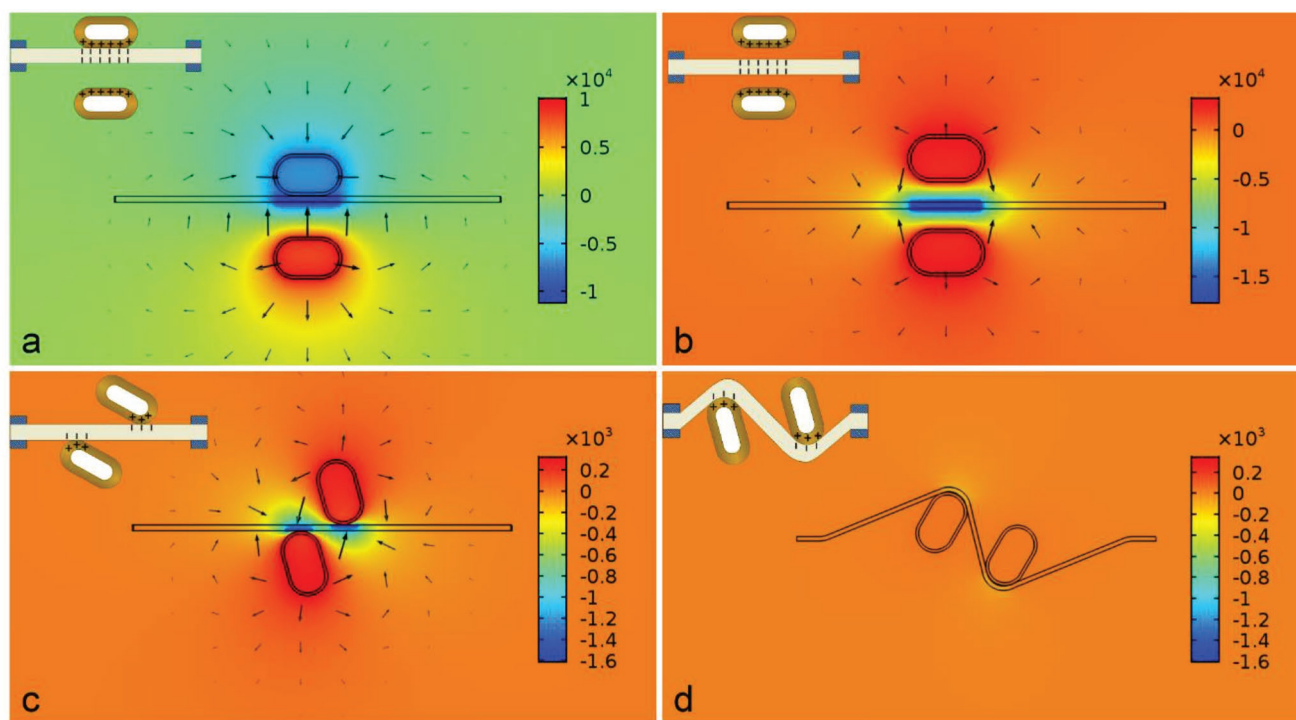
Figure 3. The potential distribution of the E-TENG under open-circuit condition based on dual contacting mode: a) one of the electrodes contacting with the rubber and b) the rubber is located at the middle of the two electrodes. The potential distribution of the E-TENG under open-circuit condition based on rotation mode: c) the two electrodes start to contact with rubber and d) the arc surfaces of the two electrodes are contacting with rubber.

the output voltage cannot be generated between the electrodes. However, the output voltage between the electrodes and ground could be utilized. In Figure 3c, the potential of the ground as the background is indicated by orange color. When the two electrodes start to contact the rubber, the negative charges on rubber could not screen the electric field of positive charges on electrodes, which leads to the high potential on electrodes. Rotating the electrodes can make the two electrodes contact the rubber more efficiently, which promotes the screening effect of the electric field (Figure 3d). The color of the electrodes is almost merging into the orange background, which suggests the output voltage (between the ground and the electrodes) is reduced. Interestingly, although the substrate of the electrodes is the insulating materials (i.e., acrylic), there was no electric field line inside, suggesting the whole electrodes including the substrates are isopotential. The explanation should be that the electrodes are conductor which would screen all outside electric field according to Gauss' law.[26]

Since the E-TENG can collect various energy in different modes, the TENG is connected to a rectifying circuit that converts AC signals of the TENG to DC, so the E-TENG can drive different devices, such as supercapacitor (SC), light-emitting diodes (LEDs), oscilloscope (OSC, DC is not necessary for it) or other electronic devices (**Figure 4**a). In Figure 4b, the E-TENG can charge a commercial supercapacitor (22 µF) directly to 50 V in around 100 s by dual contacting mode; and 25 V by single contacting mode. Then the charged supercapacitor can drive an electronic clock, inset of Figure 4b. Because the dual contacting mode has better output, it can light up 50 LEDs, as shown in Figure 4c. The brightness of LEDs at both sides is low

due to the viewing angle. When the single contacting mode was used, only 28 LEDs can be lit up. The rotational mode cannot produce larger power comparing with contacting modes, but we found it could be used as an angle sensor, as shown in Figure 2c. In Figure 4d, compared with the applied angles (21.6°, 28.9°, 36.1°, and 43.3°) denoted by yellow triangles, the measured angles (denoted by black dots, numbered from 1 to 4) well match the actual values.

In conclusion, E-TENG, which can work in various mode, dual/single contacting modes and rotation mode, was developed. Because of the elasticity of the TENG, different external stimuli with various amplitudes, directions could be used to generate electric power. Especially the dual touching mode can light 50 LEDs, and charge supercapacitor to 50 V within 100 s. The performance of single touching mode is almost 50% less compared with the dual touching mode, because the single face of the rubber is touched with the copper electrode. When the rotational mode is applied, the E-TENG can serve as an angle sensor. We trust our elastic TENG is potential to be developed as a novel self-powered source for collecting random stimuli and self-powered senor.

Experimental Section

Fabrication of the E-TENG: A 95 mm × 60 mm × 0.2 mm rubber was used as the elastic dielectric. The rubber purchased from McMaster-Carr, and the detailed product information is indicated in Table S1 (Supporting Information). The rubber was installed on a frame as shown in Figure 1a. Two copper films as electrodes were pasted on two acrylic columns, respectively. Figure S4 (Supporting Information) shows the
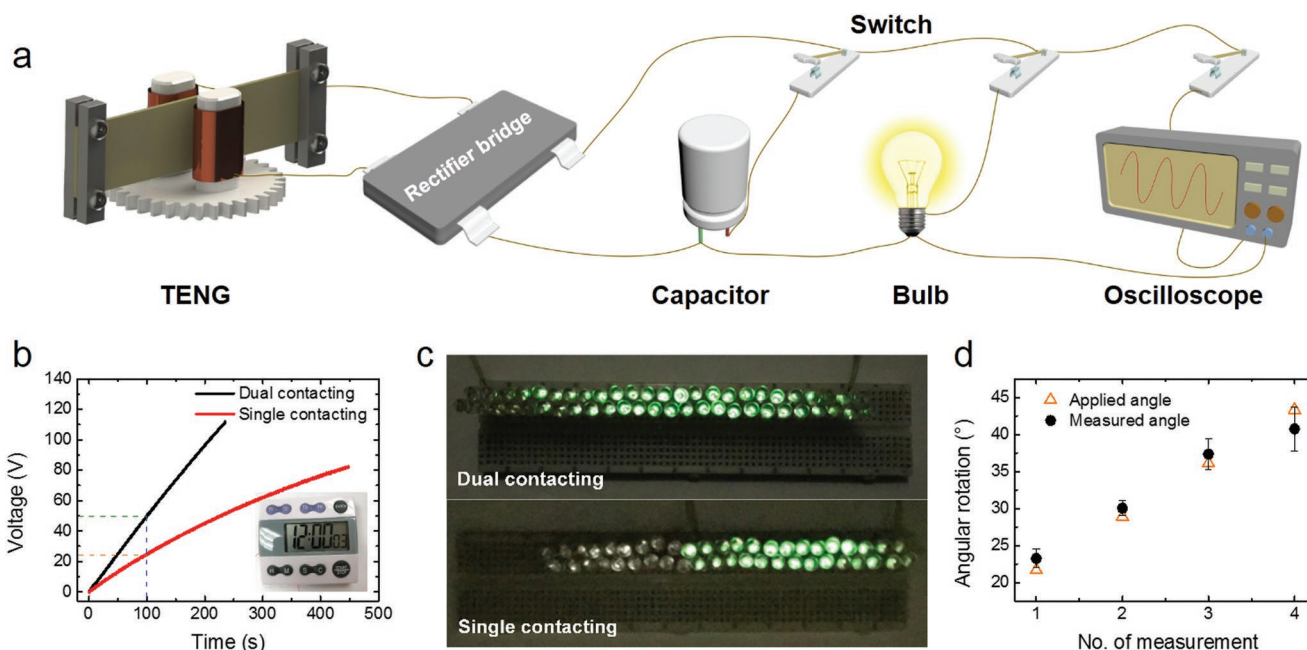
Figure 4. a) Circuit diagram of the self-charging power system integrated by the E-TENG and supercapacitor (SC), light-emitting diode (LED), and oscilloscope (OSC). b) The generated electric energy by the E-TENG based on single/dual contacting modes can charge a supercapacitor, and the stored energy can be used to drive an electronic clock as shown in the inset. c) The generated electric energy by the E-TENG based on single/dual contacting modes can light up 28/50 LEDs. d) The E-TENG being operated by rotation mode can detect the rotational angle as a sensor of angular rotations. The error bars represent standard deviation from independent measurements.

size of the column. The two columns with electrodes were fixed on a pedestal with distance 14 mm. The pedestal can uniaxial motion, and spin with respect to the center of the pedestal.

Characterization: The electric measurement was conducted by a Keithley 6514 system electrometer. A software platform programmed using LabVIEW to achieve real-time data acquisition and analysis. A commercial linear mechanical motor was used to apply external stimuli. The linear mechanical motor with connecting the pedestal controls the distance to make two (one) electrodes contact rubber can realize dual (single) contact–separation mode. In order to realize rotation mode, the rotation stimuli can be applied by the linear mechanical motor through the structure of gear (Figure S5, Supporting Information). The FEA is carried out by utilizing the COMSOL software 5.3a. The potential distribution was calculated at different states under the open-circuit condition.

Supporting Information

Supporting Information is available from the Wiley Online Library or from the author.

Conflict of Interest

The authors declare no conflict of interest.

[1] P. Erickson, M. Lazarus, G. Piggot, *Nat. Clim. Change* **2018**, *8*, 1037.
[2] C. S. Wu, A. C. Wang, W. B. Ding, H. Y. Guo, Z. L. Wang, *Adv. Energy Mater.* **2019**, *9*, 1802906.
[3] M. Xu, P. Wang, Y.-C. Wang, S. L. Zhang, A. C. Wang, C. Zhang, Z. Wang, X. Pan, Z. L. Wang, *Adv. Energy Mater.* **2018**, *8*, 1702432.
[4] J. Bae, J. Lee, S. Kim, J. Ha, B. S. Lee, Y. Park, C. Choong, J. B. Kim, Z. L. Wang, H. Y. Kim, J. J. Park, U. I. Chung, *Nat. Commun.* **2014**, *5*, 4929.
[5] W. Kim, D. Bhatia, S. Jeong, D. Choi, *Nano Energy* **2019**, *56*, 307.
[6] Y. L. Chen, Y. C. Wang, Y. Zhang, H. Y. Zou, Z. M. Lin, G. B. Zhang, C. W. Zou, Z. L. Wang, *Adv. Energy Mater.* **2018**, *8*, 1802159.
[7] Z. Lin, Z. Wu, B. Zhang, Y. C. Wang, H. Guo, G. Liu, C. Chen, Y. Chen, J. Yang, Z. L. Wang, *Adv. Mater. Technol.* **2019**, *4*, 1800360.
[8] K. Meng, J. Chen, X. Li, Y. Wu, W. Fan, Z. Zhou, Q. He, X. Wang, X. Fan, Y. Zhang, J. Yang, Z. L. Wang, *Adv. Funct. Mater.* **2019**, *29*, 1806388.
[9] S. L. Zhang, Y.-C. Lai, X. He, R. Liu, Y. Zi, Z. L. Wang, *Adv. Funct. Mater.* **2017**, *27*, 1606695.
[10] Z. L. Wang, *Faraday Discuss.* **2014**, *176*, 447.
[11] G. Zhu, C. Pan, W. Guo, C. Y. Chen, Y. Zhou, R. Yu, Z. L. Wang, *Nano Lett.* **2012**, *12*, 4960.
[12] C. Xu, Y. Zi, A. C. Wang, H. Zou, Y. Dai, X. He, P. Wang, Y. C. Wang, P. Feng, D. Li, Z. L. Wang, *Adv. Mater.* **2018**, *30*, 1706790.

[13] J. Chun, B. U. Ye, J. W. Lee, D. Choi, C. Y. Kang, S. W. Kim, Z. L. Wang, J. M. Baik, *Nat. Commun.* **2016**, *7*, 12985.

[14] L. Xu, T. Z. Bu, X. D. Yang, C. Zhang, Z. L. Wang, *Nano Energy* **2018**, *49*, 625.

[15] Y. Chen, Y. Zhang, Z. Wang, T. Zhan, Y. C. Wang, H. Zou, H. Ren, G. Zhang, C. Zou, Z. L. Wang, *Adv. Mater.* **2018**, *30*, 1803580.

[16] J. Wang, W. Ding, L. Pan, C. Wu, H. Yu, L. Yang, R. Liao, Z. L. Wang, *ACS Nano* **2018**, *12*, 3954.

[17] Z. L. Wang, *ACS Nano* **2013**, *7*, 9533.

[18] J. Yang, J. Chen, Y. Su, Q. Jing, Z. Li, F. Yi, X. Wen, Z. Wang, Z. L. Wang, *Adv. Mater.* **2015**, *27*, 1316.

[19] J. Chen, W. Tang, C. X. Lu, L. Xu, Z. W. Yang, B. D. Chen, T. Jiang, Z. L. Wang, *Appl. Phys. Lett.* **2017**, *110*, 201603.

[20] A. F. Diaz, R. M. Felix-Navarro, *J. Electrost.* **2004**, *62*, 277.

[21] S. Qi, H. Guo, J. Chen, J. Fu, C. Hu, M. Yu, Z. L. Wang, *Nanoscale* **2018**, *10*, 4745.

[22] S. L. Zhang, M. Xu, C. Zhang, Y.-C. Wang, H. Zou, X. He, Z. Wang, Z. L. Wang, *Nano Energy* **2018**, *48*, 421.

[23] S. M. Niu, S. H. Wang, L. Lin, Y. Liu, Y. S. Zhou, Y. F. Hu, Z. L. Wang, *Energy Environ. Sci.* **2013**, *6*, 3576.

[24] R. D. I. G. Dharmasena, K. D. G. I. Jayawardena, C. A. Mills, J. H. B. Deane, J. V. Anguita, R. A. Dorey, S. R. P. Silva, *Energy Environ. Sci.* **2017**, *10*, 1801.

[25] Y. Zi, S. Niu, J. Wang, Z. Wen, W. Tang, Z. L. Wang, *Nat. Commun.* **2015**, *6*, 8376.

[26] J. D. Jackson, *Classical Electrodynamics*, John Wiley & Sons, New York **1999**.